Draft version November 10, 2008
Preprint typeset using LaTeX style emulateapj v. 03/07/07

arXiv:0811.1581v1 [astro-ph] 10 Nov 2008

SPITZER OBSERVATIONS OF L429: A NEAR–COLLAPSE OR COLLAPSING STARLESS CORE

Amelia M. Stutz[1], Tyler L. Bourke[2], George H. Rieke[1], John H. Bieging[1], Karl A. Misselt[1], Philip C. Myers[2], Yancy L. Shirley[1]

Draft version November 10, 2008

ABSTRACT

We present *Spitzer* infrared observations of the starless core L429. The IR images of this core show an absorption feature, caused by the dense core material, at wavelengths ≤ 70 μm. The core has a steep density profile, and reaches $A_V > 35$ mag near the center. We show that L429 is either collapsing or in a near–collapse state.

Subject headings: ISM: globules – ISM: individual (LDN 429) – infrared: ISM – (ISM:) dust, extinction

1. INTRODUCTION

The collapse of a dense cloud core into a star happens rapidly (Hayashi 1966) and therefore is rarely observed; furthermore, most dense cores appear not to be collapsing but to be close to equilibrium (e.g., Lada et al. 2008). If they are not sufficiently supported by gas pressure and turbulence, then a plausible level of magnetic field strength would suffice to support them (e.g., Kandori et al. 2005; Stutz et al. 2007; Alves et al. 2008). Because the process of collapse is so rarely observed, there is considerable debate about what triggers it and how it proceeds to form a star. Additional examples of dense cores in extreme states that indicate either collapse or a condition just prior to collapse are critical to constrain theories about the first stages of star formation.

Mm-wave line observations are the traditional means to search for collapsing cloud cores, such as in the pioneering study by Walker et al. (1986). The subsequent discussion (e.g., Menten et al. 1987; Walker et al. 1988; Wootten 1989; Mundy et al. 1990; Narayanan et al. 1998) illustrates the ambiguities in the interpretation of velocity data in star forming dense cores. Alternative observational approaches are necessary to supplement such line measurements and provide a better understanding of collapsing and nearly-collapsing dense cores.

In this paper we characterize the structure of the extremely dense core L429, using the infrared shadow technique we have demonstrated on two other globules (Stutz et al. 2007, 2008). This core is already known to have an extremely high deuterium fraction, believed to be an indication of its being very close to collapsing into a protostar, and a low internal temperature of only $T_{\rm kin} \sim 8$ K, reducing pressure support to low levels (Bacmann et al. 2003; Crapsi et al. 2005). Bacmann et al. (2000) detected a 7 μm shadow from L429 using ISOCAM. Here, we report that this shadow is so opaque that it is detectable at 70 μm. The presence of significant absorption at this long wavelength demonstrates that L429 is indeed extremely dense. Our analysis of the shadow also demonstrates that it is very compact with a steep density gradient. We show how these characteristics put L429 in the collapsing or near–collapsing starless core category.

2. OBSERVATIONS AND PROCESSING

L429 was observed by *Spitzer* using MIPS, program ID 30384, P.I. Tyler L. Bourke, and with the IRAC instrument, program ID 20386, P.I. Philip C. Myers. The MIPS observations utilized scan map mode in all three bands. The data reductions were carried out as described in Stutz et al. (2007). The MIPS images are $\sim 15\overset{\prime}{.}5 \times 54'$ in size, with exposure times of ~ 150 s at 24 μm, ~ 60 s at 70 μm, and ~ 15 s at 160 μm. For the 70 μm and 24 μm data respectively the beam size is $\sim 18''$ and $\sim 6''$, the nominal default pixel scale is $9\overset{\prime\prime}{.}8$ and $2\overset{\prime\prime}{.}5$, and the pixel scale in our images is $4''$ and $1\overset{\prime\prime}{.}24$. The IRAC reductions were carried out as described in Harvey et al. (2006). The IRAC images are $\sim 6' \times 5\overset{\prime}{.}5$ in size, with exposure times of ~ 800 s. The *Spitzer* data are shown in Figure 1. We also use the 2MASS All–Sky Point Source Catalog (PSC) (Skrutskie et al. 2006) photometry for two well–detected sources within $40''$ of the center of L429Reddening estimates for these sources, assuming the Rieke & Lebofsky (1985) extinction levels, are plotted in Figure 2.

3. THE DISTANCE

The commonly accepted distance to L429 is 200 pc (e.g., Lee et al. 1999; Bacmann et al. 2000; Crapsi et al. 2005), based on the likely association of this cloud with the Aquila Rift. Dame & Thaddeus (1985) find a distance to the Aquila Rift based on the CO line $V_{\rm LSR} = 8$ km s^{-1}. They summarize the results of various studies and conclude that the distance to the Aquila Rift is consistent with 200 ± 100 pc. More recently, Straižys et al. (2003) derive a distance to the near side of the Rift of 225 ± 55 pc, while Kawamura et al. (2001) derive a distance to an Aquila cloud complex centered at $\sim l = 48°$ and $\sim b = -6°$ of 230 ± 30 pc, both consistent with previous studies. The depth of the absorption feature (see Fig. 1) implies that L429 must lie on the near side of, or in front of, the Aquila Rift because substantial amounts of foreground material would be warmed by the interstellar radiation field and would dilute the shadow. We assume a distance of 200 pc, consistent with previous distance determinations. If the distance to L429 is larger the derived mass will increase, making the core less stable and more likely to be collapsing.

4. SHADOW PROFILES

---

[1] Steward Observatory, University of Arizona, 933 North Cherry Avenue, Tucson, Arizona 85721; astutz@as.arizona.edu.
[2] Harvard-Smithsonian Center for Astrophysics, 60 Garden Street, Cambridge, MA 02138

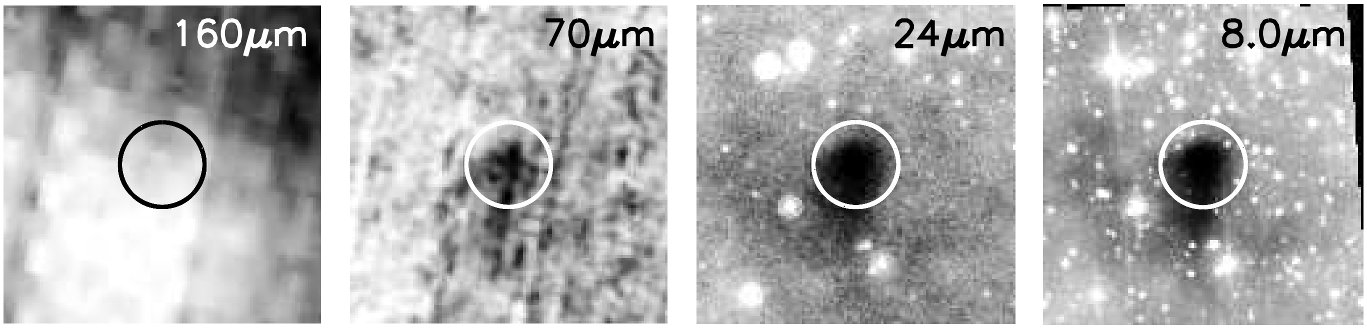

FIG. 1.— MIPS and IRAC $5' \times 5'$ images of L429 centered at RA = $18^h17^m05.4^s$, Dec = $-08°13'32.3''$ (J2000; $l = 21.68°$, $b = 3.80°$). The circle (radius = $40''$) indicates the location of the shadow produced by the dense core material. The images are displayed on a log scale; north is up and east is to the left.

L429 is seen in absorption at $\lambda \leq 70$ μm; at 160 μm there is large-scale emission but no isolated local peak is observed (see Fig. 1). In addition, no compact emission source is detected at any *Spitzer* wavelength within the shadow, and so no source of luminosity $\gtrsim 10^{-3}$ $L_\odot$ is present (Harvey et al. 2006; Dunham et al. 2008). We derive extinction profiles from the observed shadows at 70, 25, 8.0, and 5.8 μm using techniques similar to those discussed in detail in Stutz et al. (2007, 2008).

4.1. *70 μm profile*

The first step in deriving the 70 μm profile is to subtract from the image a value that represents zodiacal emission and other foreground sources. For L429 the shadow is the darkest part of the image. For this reason the image zero level cannot be determined directly from the image itself. To set an upper limit on the optical depth, we zero the image using the lowest pixel value in a $44'' \times 44''$ box centered on the shadow; in this case the zero value is ~ 5.2 MJy sr^{-1} below the mean pixel flux level immediately outside the shadow. Ideally, one would compute the minimum value based on more pixels. However, the 70 μm pixel size is a non-negligible fraction of the size of the core of absorption feature; taking more pixels would dilute the depth of the shadow. We use IRAS data to set the lower limit on the optical depth profile: we measure the flux level outside the shadow to be ~ 13.5 MJy sr^{-1} above the foreground component of emission, interpolated to 70 μm from the 60 and 100 μm IRAS images and estimated far away from regions with significant emission (about 4.5° away). For this value, the minimum shadow value is 8.3 MJy sr^{-1} above the image zero level. This zero level is a very conservative estimate because the shadow region is surrounded by high levels of emission which are very likely to raise the foreground contribution above the level we use here. This lower limit also accounts for the MIPS 70 μm calibration error, 5% (Gordon et al. 2007), and the IRAS extended source calibration error, which can be as large as 30% (Wheelock et al. 1994).

After zeroing the image we mask out all pixels with possible emission above the sky level. The mask threshold is set to the mean value plus 0.5σ measured for pixels in a $4' \times 4'$ region $4'$ north of the shadow. Next we measure the mean pixel values, termed f here, in nested, and concentric, circular regions, with radii starting at $7''.5$ and increasing in $5''$ steps, out to $\sim 120''$, centered at RA = $18^h17^m05.4^s$, Dec = $-08°13'32.3''$ (J2000), without accounting for fractions of pixels. We ignore all pixels in the southern half of the shadow because the shadow has a tail extending to the south and the assumption of spherical symmetry breaks down (see Figure 1). Finally, to determine the optical depth at 70 μm, $\tau_{70} = -ln(f/f_0)$, we average profile values at radii $> 27''.5$ to measure f_0, the intrinsic, unobscured local flux value. The outer radius of the core at 70 μm, equal to $27.5''$, is set by the observed flattening of the measured flux profile at that radius, indicating that there is little to no absorption at larger radii. Following Stutz et al. (2007), we derive the 70 μm A_V profile shown in Figure 2 with open triangles: downward–pointing triangles represent the upper limit and the upward–pointing triangles represent the lower limit. The innermost region has an optical depth of $\tau_{70} = 1.8$ to 0.46 (upper and lower limits). The total mass (gas plus dust) implied by the 70 μm profile is given by

$$M_{70} = 5.1\ M_\odot \left(\frac{D}{200\ \mathrm{pc}}\right)^2 \frac{1.58 \times 10^2\ \mathrm{cm}^2\ \mathrm{gm}^{-1}}{\kappa_{\mathrm{abs},70}}, \quad (1)$$

where we have assumed a gas to dust mass ratio of 100 and the Ossenkopf & Henning (1994) model dust opacity for coagulated dust grains of 1.58×10^2 cm^2 gm^{-1}. The value of 5.1 M$_\odot$ is the *upper limit* on the mass; the *lower limit* mass is 1.6 M$_\odot$. The enclosed mass profile is shown in Fig. 3. As noted earlier, our limits on τ are very conservative. We performed an error analysis to measure the effect of a reasonable perturbation in the assumed zero level and the calculated value for f_0 and find that the errors are absorbed into the limits by a wide margin. For a dust opacity of $\kappa_{\mathrm{abs},70} = 6.35 \times 10^1$ cm^2 gm^{-1}, from the $R_V = 5.5$ model from Draine (2003a,b), we calculate a 70 μm mass of $M_{70} = 12.6 - 4.0$ M$_\odot$.

4.2. *24, 8.0, and 5.8 μm profiles*

The method used to derive the shorter wavelength profiles is essentially the same as described above. First, we zero the images using the darkest pixel in the shadow. Second, the mask threshold is determined from the pixel value distribution in the sky region. We measure the mean pixel value in circular regions starting with a radius of $2''.5$ and increasing in steps of $2''.5$, out to a radius $\sim 120''$. The value of f_0 is determined by averaging pixel values between radii of $40''$ and $45''$. These radii were chosen based on a flattening of the 24 μm profile in this region. At radii between $45''$ and $\sim 55''$ the profile continues to rise, likely due to contamination from other

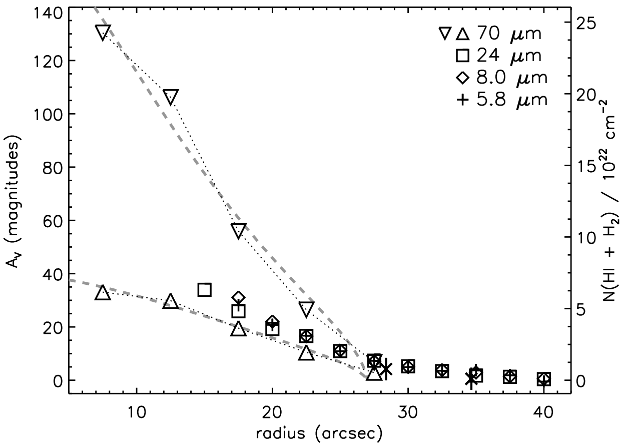

FIG. 2.— Extinction profiles for L429. The downward– and upward–pointing triangles (connected with a dotted line) represent upper and lower bounds on the 70 μm extinction profile, respectively; the innermost 70 μm region has an optical depth of $\tau_{70} = 1.8$ to 0.5, for the upper and lower bounds, respectively. The dashed lines represent the Bonnor-Ebert best-fit models for the 70 μm extinction profile derived assuming a distance of 200 pc; both models require high temperatures that are in contradiction with the observations (see § 5). The 24 μm (squares), 8.0 μm (diamonds), and 5.8 μm (plus signs) profiles are scaled to match the outer two radial regions of the 70 μm profile; for these three profiles we only show points with $\tau < 1.0$. The crosses (×) are 2MASS extinction measurements for two sources with reliable detections. We assume Ossenkopf & Henning (1994) dust opacities for the extinction profiles (see § 4).

nearby sources. Using larger values of f_0 would artificially increase τ. This choice of f_0 is further justified by the 8.0 and 5.8 μm profiles: they show an increase in the mean pixel value well past $40''$ but a decreasing value approaching the inner estimate at radii larger than $\sim 80''$, and by a radius of $\sim 100''$ the profiles match the inner values. This increase in the profile values at intermediate radii may be caused by limb brightening of the core as it is irradiated by the interstellar radiation field. If the emission raises the observed shadow flux then it will cause an underestimate of τ at all wavelengths; however, if it predominantly increases the unobscured flux levels outside the shadow τ will be over–estimated. We do not attempt to correct for this effect. We calculate optical depth limits of $\tau_{24} = 2.1, \tau_{8.0} = 3.2$ and $\tau_{5.8} = 2.2$ through the center of the profiles. The implied total masses at these wavelengths is ~ 1.2 M$_\odot$ for all three profiles, assuming Ossenkopf & Henning (1994) model dust opacities. The discrepancy between this mass and the 70 μm mass (between 1.6 and 5.1 M$_\odot$) most likely results from the high optical depth in the core. If the core is dense enough to be observed in absorption at 70 μm then it is certainly opaque at shorter wavelengths; the A_V profile and mass estimates at shorter wavelengths will be lower limits. In the CB190 case the core was observed in absorption at 24 μm but not at 70 μm, and the maximum measured extinction value was $A_V \sim 30$ mag ($\tau_{24} = 1.4$), much smaller than the values measured here (Stutz et al. 2007). Therefore we reject all 24, 8.0, and 5.8 μm $\tau > 1.0$ points and we scale the profiles to match the 70 μm extinction values at the outer two 70 μm radii. In Figure 2 we plot the scaled profiles; the shapes of the profiles match well.

5. DISCUSSION

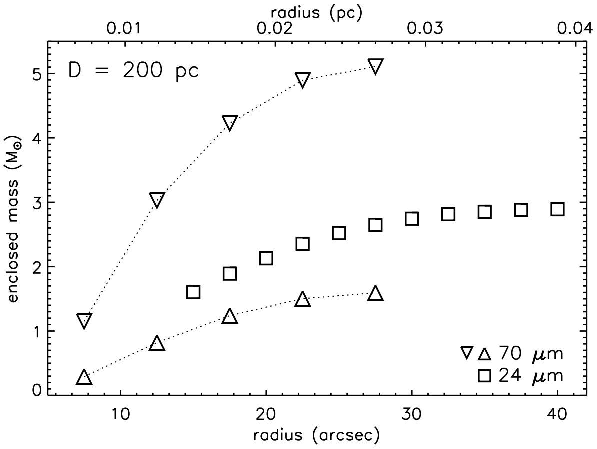

FIG. 3.— Enclosed mass vs. radius for L429 calculated assuming a distance of 200 pc. The downward– and upward–pointing triangles represent masses calculated using the upper and lower bounds on the 70 μm extinction profiles, respectively. The 24 μm masses (squares) are scaled to match the 70 μm profile; we only show 24 μm points with $\tau < 1.0$. We assume Ossenkopf & Henning (1994) dust opacities (see §4).

Bonnor-Ebert models are often used to characterize starless cores; these models generally fit the observed density profiles with reasonable fidelity (e.g., Kandori et al. 2005; Shirley et al. 2005; Stutz et al. 2007). Bonnor-Ebert models describe a self–gravitating pressure confined isothermal sphere in hydrostatic equilibrium. The density profiles are described by three parameters: temperature, central density ρ_c (or equivalently, $\xi_{\max}$), and the outer radius of the cloud. A model will be unstable to collapse if $\xi_{\max} > 6.5$. We fit said models to the extinction profiles discussed above. We use a 3D grid of models in temperature, radius, and $\xi_{\max}$; see Stutz et al. (2007) for a more detailed discussion of the models and the fitting method. One strong constraint in interpreting the best–fit models is that L429 is dark at $\lambda \lesssim 70$ μm, and therefore the temperature cannot be greater than ~ 12 K, in agreement with other core temperature measurements (e.g., Lemme et al. 1996; Bacmann et al. 2002; Hotzel et al. 2002; Kirk et al. 2007). The best–fit models for the upper and lower bounds on the 70 μm profile are shown in Figure 2 as grey dashed lines. The 70 μm profile has a best–fit temperature of $T = 56 - 130$ K, for the upper and lower bounds, respectively; these temperatures are in clear contradiction with the data. The best–fit outer radius is $27''$, for both the upper and the lower limit, and the best–fit $\xi_{\max} = 4.5$ and 3.0, for the upper and lower limit respectively. As the assumed distance is increased (in this case to 270 pc) the best–fit models become even more implausible, with temperatures always > 70 K. At a distance of 100 pc the best–fit temperatures are $T = 26 - 90$ K, still in contradiction with the data. These high temperatures indicate that L429 requires additional support (turbulence and magnetic fields) beyond thermal to prevent collapse.

Crapsi et al. (2005) observe N_2D^+ and N_2H^+ line widths $\sim 0.3 - 0.4$ km s^{-1} and calculate excitation temperatures $T_{\rm ex} \sim 4.5 - 5$ K. The particle of mean molecular mass has velocity FWHM ~ 0.4 km s^{-1} for temperature 8 K, indicating that the turbulent energy contribution to the support in L429 is only comparable to the thermal contribution (Hotzel et al. 2002).

Magnetic fields are a possible source of support in starless cores. Inferred magnetic field strengths in cores range from, e.g., $\lesssim 15$ μG to 160 μG (Bergin & Tafalla 2007). For $\theta = 30''$, a distance of 200 pc, and $B = 160$ μG, the mass that can be supported is $M_{\rm B} = 1$ M$_\odot$ (Stahler & Palla 2005). Furthermore, from equation 1 and the Stahler & Palla (2005) analysis, the condition of stability requires a minimum magnetic field strength of:

$$B = 861\,\mu{\rm G}\left(\frac{1.58\times10^{2}\ {\rm cm}^{2}\ {\rm gm}^{-1}}{\kappa_{\rm abs,70}}\right)\left(\frac{M_{\rm B}}{M_{70}}\right)\left(\frac{\theta}{30''}\right)^{-2},$$

where θ is the angular radius of the core. The mean column density of the 70 μm profile is $\langle N({\rm H_2})\rangle \simeq 1.1 \times 10^{23}$ cm^{-2}; given this column, the correlation presented by Basu (2004) implies a line-of-sight magnetic field of $B_{\rm los} = 250$ μG; we estimate the total field as $B_{\rm tot} = \sqrt{3} \times B_{los} = 430$ μG, although this relation has large scatter.

Although the field required to support L429 is larger than expected, our understanding of the limits on magnetic field strengths does not allow for a strong constraint. In addition to requiring a field exceeding the likely range of values, supporting the globule entirely with magnetic pressure has other consequences. One might expect asymmetries to develop, given the asymmetric pressure provided by magnetism. If such structures can be avoided (Shu et al. 1987), another issue is that the field should leak out of the globule by ambipolar diffusion, on timescales $\sim 3 \times 10^6$ yr (Stahler & Palla 2005). Thus, either the field is already too small to prevent the collapse of the globule, or the collapse will only be delayed for a time.

If infall is occurring in L429, the observed line width is very narrow. Crapsi et al. (2005) detect a double-peaked N_2H^+ $(1-0)$ line and Lee et al. (1999) detect a double-peaked CS $(2-1)$ line, both measurements with roughly equal brightness in the blue and red peaks. Lee et al. (1999) state that because other thin tracers show single Gaussian components, the observed double peak is likely due to self absorption at high optical depth; these authors also note that L429 is one of two sources out of 163 spectra that show small wing components. Lee et al. (2004) classify L429 as a possible infall candidate based on their observation of CS $(3-2)$, which has a double peaked profile with more emission in the blue peak. Sohn et al. (2007) also measure a double peaked profile in HCN $(1-0)$; they note that this source is one of two (out of 85 cores surveyed) that has some line strength anomalies in the three hyperfine HCN lines. Recently, Caselli et al. (2008) have found that L429 has a large amount of ortho-$H_2D^+(1_{1,0}$–$1_{1,1})$ emission, which they find to be correlated with increased central concentration, CO depletion, and deuteration, providing further evidence that L429 is very evolved.

6. CONCLUSIONS

We measure the density profile of L429 from the 70 μm absorption feature observed with the *Spitzer* Telescope. We conclude that:

1. The strong absorption even at 70 μm indicates that L429 is exceptionally dense.
2. At the same time, the absorbing cloud is very compact and has a very steep density gradient (as seen most clearly at 24 μm).
3. The temperature can be no more than 12 K.
4. As a result of these extreme characteristics, thermal pressure fails, by a wide margin, to support the globule; turbulent support is also inadequate by a wide margin.
5. The magnetic field required to make up the rest of the required pressure for support would be surprisingly large; even if present, such a large field will leak out of the globule through ambipolar diffusion.
6. Therefore, L429 is either already undergoing collapse or is approaching an unstable, near-collapse state.

We thank the referee for their helpful comments. Support for this work was provided through NASA contracts issued by Caltech/JPL to the University of Arizona (1255094) and to SAO (1279198 and 1288806). This work was also supported by the National Science Foundation grant AST-0708131 to The University of Arizona.

REFERENCES

Alves, F. O., Franco, G. A. P., & Girart, J. M. 2008, A&A, 486, L13
Bacmann, A., André, P., Puget, J.-L., Abergel, A., Bontemps, S., & Ward-Thompson, D. 2000, A&A, 361, 555
Bacmann, A., Lefloch, B., Ceccarelli, C., Castets, A., Steinacker, J., & Loinard, L. 2002, A&A, 389, L6
Bacmann, A., Lefloch, B., Ceccarelli, C., Steinacker, J., Castets, A., & Loinard, L. 2003, ApJ, 585, L55
Basu, S. 2004, in Young Local Universe, Proceedings of XXXIXth Rencontres de Moriond, eds. A. Chalabaev, T. Fukui, T. Montmerle, and J. Tran-Thanh-Van. Paris: Editions Frontieres, ArXiv Astrophysics e-prints, arXiv:astro-ph/0410534
Bergin, E. A., & Tafalla, M. 2007, ARA&A, 45, 339
Caselli, P., Vastel, C., Ceccarelli, C., van der Tak, F., Crapsi, A., & Bacmann, A. 2008, arXiv:0809.2803
Crapsi, A., Caselli, P., Walmsley, C. M., Myers, P. C., Tafalla, M., Lee, C. W., & Bourke, T. L. 2005, ApJ, 619, 379
Dame, T. M., & Thaddeus, P. 1985, ApJ, 297, 751
Draine, B. T. 2003a, ARA&A, 41, 241
Draine, B. T. 2003b, ApJ, 598, 1017
Dunham, M. M., Crapsi, A., Evans, N. J., II, Bourke, T. L., Huard, T. L., Myers, P. C., & Kauffmann, J. 2008, ArXiv e-prints, 806, arXiv:0806.1754
Gordon, K. D., et al. 2007, PASP, 119, 1019
Harvey, P. M., et al. 2006, ApJ, 644, 307
Hayashi, C. 1966, ARA&A, 4, 171
Hotzel, S., Harju, J., & Juvela, M. 2002, A&A, 395, L5
Kandori, R., et al. 2005, AJ, 130, 2166
Kawamura, A., Kun, M., Onishi, T., Vavrek, R., Domsa, I., Mizuno, A., & Fukui, Y. 2001, PASJ, 53, 1097
Kirk, J. M., Ward-Thompson, D., & André, P. 2007, MNRAS, 375, 843
Lada, C. J., Muench, A. A., Rathborne, J., Alves, J. F., & Lombardi, M. 2008, ApJ, 672, 410
Lee, C. W., Myers, P. C., & Tafalla, M. 1999, ApJ, 526, 788
Lee, C. W., Myers, P. C., & Plume, R. 2004, ApJS, 153, 523
Lemme, C., Wilson, T. L., Tieftrunk, A. R., & Henkel, C. 1996, A&A, 312, 585
Menten, K. M., Serabyn, E., Guesten, R., & Wilson, T. L. 1987, A&A, 177, L57
Mundy, L. G., Wootten, H. A., & Wilking, B. A. 1990, ApJ, 352, 159
Narayanan, G., Walker, C. K., & Buckley, H. D. 1998, ApJ, 496, 292
Park, Y.-S., Lee, C. W., & Myers, P. C. 2004, ApJS, 152, 81
Ossenkopf, V., & Henning, T. 1994, A&A, 291, 943
Rieke, G. H., & Lebofsky, M. J. 1985, ApJ, 288, 618

Shirley, Y. L., Nordhaus, M. K., Grcevich, J. M., Evans, N. J., Rawlings, J. M. C., & Tatematsu, K. 2005, ApJ, 632

Shu, F. H., Adams, F. C., & Lizano, S. 1987, ARA&A, 25, 23

Sohn, J., Lee, C. W., Park, Y.-S., Lee, H. M., Myers, P. C., & Lee, Y. 2007, ApJ, 664, 928

Skrutskie, M. F., et al. 2006, AJ, 131, 1163

Stahler, S. W., & Palla, F. 2005, The Formation of Stars, by Steven W. Stahler, Francesco Palla, pp. 865. ISBN 3-527-40559-3. Wiley-VCH , January 2005

Straižys, V., Černis, K., & Bartašiūtė, S. 2003, A&A, 405, 585

Stutz, A. M., et al. 2007, ApJ, 665, 466

Stutz, A. M., et al. 2008, ArXiv e-prints, 807, arXiv:0807.2241, ApJin press.

Walker, C. K., Lada, C. J., Young, E. T., Maloney, P. R., & Wilking, B. A. 1986, ApJ, 309, L47

Walker, C. K., Lada, C. J., Young, E. T., & Margulis, M. 1988, ApJ, 332, 335

Walker, C. K., Narayanan, G., & Boss, A. P. 1994, ApJ, 431, 767

Wheelock, S. L., et al. 1994, NASA STI/Recon Technical Report N, 95, 22539

Wootten, A. 1989, ApJ, 337, 858